Pore connectivity of alumina and aluminium borate from nitrogen isotherms

Chung-Kung Lee[a]* and Cherng-Shyan Tsay[b]

[a] *Department of Environmental Engineering, Van-Nung Institute of Technology, Chung-Li, 32054, Taiwan, Republic of China*

[b] *Department of Chemical Engineering, National Central University, Chung-Li, 32054, Taiwan, Republic of China*

The effects of calcination temperature on the connectivity of pore networks of alumina and aluminium borate samples, prepared by coprecipitation methods and low-water sol–gel processes, have been investigated based on the percolation analysis of their nitrogen adsorption isotherms. The mean coordination number (Z) was determined with the aid of the recently proposed Seaton theory. Values of Z obtained with this method cover the range 2–3, implying a low connection of pores in all the examined porous samples. Thermal effects may increase or decrease Z values depending on the samples. On the other hand, Z values of aluminium borate samples obtained from the coprecipitation method were slightly larger than those from the sol–gel process. It was also found that for sol–gel processed samples, Z values of alumina were slightly larger than that of aluminium borate.

1 Introduction

It is well known that the macroscopic properties of solid materials are closely connected to their porous microstructure, which is usually characterized by quantities such as density, surface area, porosity, pore size, pore size distribution (PSD), pore geometry and topology. These common terms used to describe the microstructure of a porous material are in fact parameters related to certain macroscopic measurements. Many techniques have been applied to characterize porous solids. They range from simple pycnometry, gas adsorption, fluid penetration and calorimetric measurements, to the more recent radiation scattering, xenon NMR, size exclusion chromatography or ultrasonic methods.[1] Among these techniques, gas adsorption is the most popular for the characterization of porous solids. From the standard nitrogen isotherms, values such as total pore volume, BET surface area and PSD can be obtained. However, more information can still be extracted if new theories are adopted. Among them is percolation analysis, which pays special attention to the connectivity of the pore system and its relation to the adsorption–desorption hysteresis loop.[2]

Percolation means spreading or penetration from one side of the system to another. It is appropriate to describe how the connectivity of a system affects its macroscopic properties. Since the observed hysteresis in nitrogen isotherms may be related to the topology of the pore network, the natural language to describe this phenomenon is percolation theory. The mapping between adsorption hysteresis and the percolation process has been employed previously by several authors to extract structural information from adsorption data.[2] Taking the desorption isotherm as a bond percolation phenomenon and the assumption that pore network effects dominate, *i.e.*, the thermodynamic contribution to the observed hysteresis is neglected, Seaton and co-workers[3–7] have proposed a method to determine the mean coordination number of the pore network, Z, and the characteristic size of the particles, L, expressed as the number of pore lengths.

The procedures for the determination of Z and L from the experimental adsorption data can be summarized as follows:[3] first, the PSD is obtained using the method of Barrett *et al.*[8] with a cylindrical pore model. Then, the bond occupation probability f is obtained as a function of percolation probability F from the adsorption and desorption isotherms, using the PSD obtained above as an input. Finally, the best Z and L values are obtained by fitting the experimental scaling data (F, f) obtained above to a generalized scaling relation between F and f. For a detailed description one may refer to the work of Seaton.[3] In our analysis, the generalized scaling relation

$$L^{\beta/\nu}ZF = G[(Zf - 3/2)L^{1/\nu}]$$

where the critical exponents β and ν have values of 0.41 and 0.88, respectively, was constructed using the simulation data of Kirkpatrick.[9]

For this analysis, some further comments are in order. (1) It gives information only about the network of micro- and mesopores. No structural information about macropores can be obtained since no nitrogen condenses in macropores during the adsorption process. (2) It is suitable for the IUPAC type H1 and H2 loops and is difficult to use for analysis of H3 and H4 loops. (3) Only the data points where F is significantly different from zero and from f can be used in the fitting procedure. The other points are far away from the percolation threshold and are therefore outside the range of validity of the generalized scaling relationship. (4) Although a mean coordination number is obtained, no information about the distribution of coordination number within the pore network is available.

Alumina gel is technically an important porous material. Apart from conventional applications as adsorbent and catalyst support, many potential new usages of this oxide have been proposed in electronics, optics and other advanced fields.[10–14] For these practical applications, it was found that the microstructure of such porous oxides may play a key role in determination of their macroscopic characteristics. One example is when used as adsorbents and catalyst supports, both the geometry (the shape and distribution of size) and connectivity of the pore space are critical for the transport or reaction behavior in such porous materials. However, the structure and physical properties of these porous oxides depend strongly on the synthetic conditions and processes as

well as treatment temperature. For the former, two examples are the incorporation of boron into the alumina structure which may increase the surface area[15] and sol–gel processing which can produce very porous (>90%) alumina xerogels with small and narrowly distributed pores.[16] For the latter, the examination of time–temperature evolution of some alumina and aluminium borate samples by nitrogen adsorption, transmission electron microscopy, thermal analysis, IR absorption and X-ray techniques[17–21] indicated that thermal effects can strongly affect the microstructure of such materials. In this study, effects of calcination temperature and synthesis processes (coprecipitation method and sol–gel process) on the pore connectivity of alumina and aluminium borate will be examined through the percolation analysis of some carefully measured nitrogen isotherms.

2   Experimental

The aluminium borate mixed oxide derived by the coprecipitation process was synthesized according to the procedure outlined by Peil et al.[21] Aluminium nitrate $[Al(NO_3)_3 \cdot 9H_2O$, 98.5%, Merck] and boric acid $(H_3BO_3$, >99.8%, Merck) were mixed with $B/Al = 1/9$ and the pH was controlled to close to 2 by deionized water. An ammonia solution (pH = 11.5) was used as precipitant for the aluminium–borate solution in the coprecipitation process. The two solutions were slowly added into a third container with deionized water to maintain a constant pH of 9. The resulting precipitate was filtered, washed with deionized water (three times), oven-dried at 100 °C for 24 h, and then calcined at different temperatures for 4 h. The alumina was synthesized with a similar process except for the absence of boric acid.

The sol–gel process derived aluminium borate xerogel was prepared from a low-water non-aqueous sol synthesized from aluminum tri-sec-butylate $\{Al[OCH(CH_3)C_2H_5]_3$ (ATSB), 97%, Merck}, tributyl borate $\{B[CH_3(CH_2)_3O]_3$ (TB), 99%, Aldrich}, absolute ethanol $(C_2H_5OH$, >99.8%, Merck), deionized water and nitric acid $(HNO_3$, 65%, Merck). The molar ratio of ATSB, TB, H_2O, EtOH and HNO_3 used is $0.1 : 0.0111 : 0.025 : 10 : 0.0065$, where the water to alkoxide ratio is only half that suggested by Yoldas.[22]

Initially, 0.0111 mol TB was mixed with 10 mol absolute ethanol in a round bottomed flask, then heated to 80 °C on a heating mantle, and stirred vigorously with an electric stirrer. Preheated water (0.0125 mol) and HNO_3 (0.003 mol) were added and the flask contents were continually refluxed for 1 h. ATSB (0.1 mol) was then added with vigorous stirring. After the addition of a preheated mixture of additional water (0.0125 mol) and HNO_3 (0.0035 mol), the contents in the flask were stirred under the same conditions for 4 h. When the obtained sol was cooled to room temperature, it formed a gel in ca. 70 h in a 70% filled and tightly sealed 100 ml beaker. The glassy gel was dried at 110 °C for 10 h, and calcined to the desired temperature with a heating rate of 60 °C h^{-1} and a final holding time of 4 h. At ca. 500 °C the xerogel turned dark brownish due to carbonization of organic residues. This color disappeared at ca. 700 °C as the carbon was burned off. The alumina xerogel was synthesized by a similar process except for the absence of TB.[23]

We denote the coprecipitation method derived alumina and aluminium borate as C10A and C9A1B while the sol–gel derived counterparts are denoted S10A and S9A1B, respectively.

XRD patterns of the calcined samples were measured on a Siemens D-500 instrument with Cu-Kα radiation (30 mA and 40 kV). Nitrogen adsorption isotherm and desorption hysteresis loops were measured at 77 K with a Micromeritics ASAP-2000 instrument. All samples were outgassed at 350 °C for 24 h before adsorption measurements.

3   Results and Discussion

In our analysis of the nitrogen isotherms, we strive to identify a key parameter which can provide an adequate characterization of the pore network of alumina and aluminium borate gels for a wide variety of calcination temperatures. The porous microstructure of solid materials is usually characterized from the nitrogen isotherm by parameters such as BET surface area, pore size and PSD. However, there is yet more information one can extract from the isotherms, for instance percolation analysis can give a measure of the connectivity of the pores. Below we first give basic structural information of alumina and aluminium borate gels obtained from nitrogen isotherms.

3.1   Surface area, pore size and PSD

Fig.1 shows the nitrogen adsorption–desorption isotherms we have measured on the alumina and aluminium borate gels calcined at different temperatures. Some key features are seen directly from Fig. 1. The monolayer capacity, and thus the BET surface area, decreases with increasing calcination temperature. Also evident is that the BET surface areas of samples from sol–gel processing are slightly larger than those obtained from coprecipitation at low calcination temperatures. The incorporation of boron into the alumina structure using the sol–gel process leads to a slight increase in the surface area.

All adsorption isotherms except for samples calcined at 1250 °C exhibited obvious capillary condensation at an intermediate relative pressure. The isotherms for the 1250 °C samples showed virtually no uptake until close to saturation pressure, where capillary condensation in the few large voids between α-alumina crystalline grains started. Owing to the increase of condensation pressure with increasing calcination temperature, thermal effects may increase the mean pore size. The PSDs calculated from the capillary condensation model are shown in Fig. 2. As demonstrated in Fig. 2(b) and (d), the
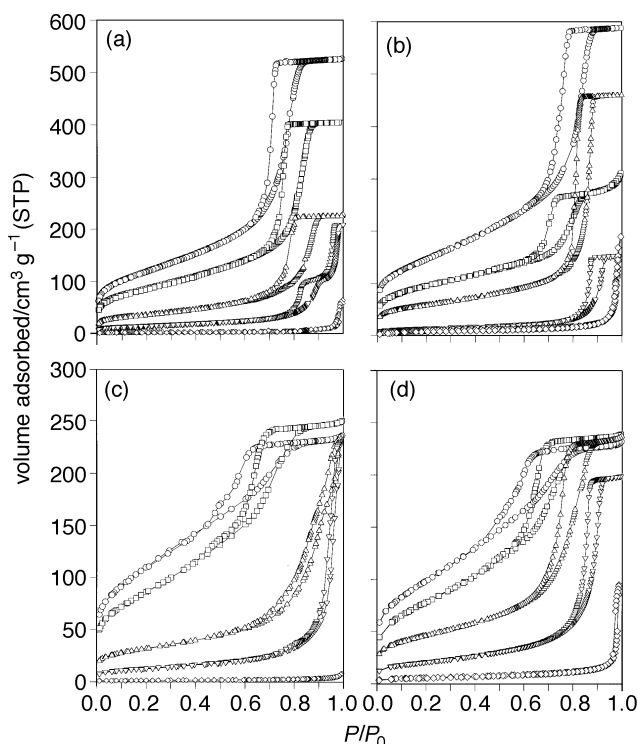

Fig. 1 Nitrogen adsorption isotherms of (a) S10A, (b) S9A1B, (c) C10A and (d) C9A1B calcined at different temperatures; (○) 500, (□) 700, (△) 900, (▽) 1100 for (a) but 1000 for (b)–(d), and (◇) 1250 °C
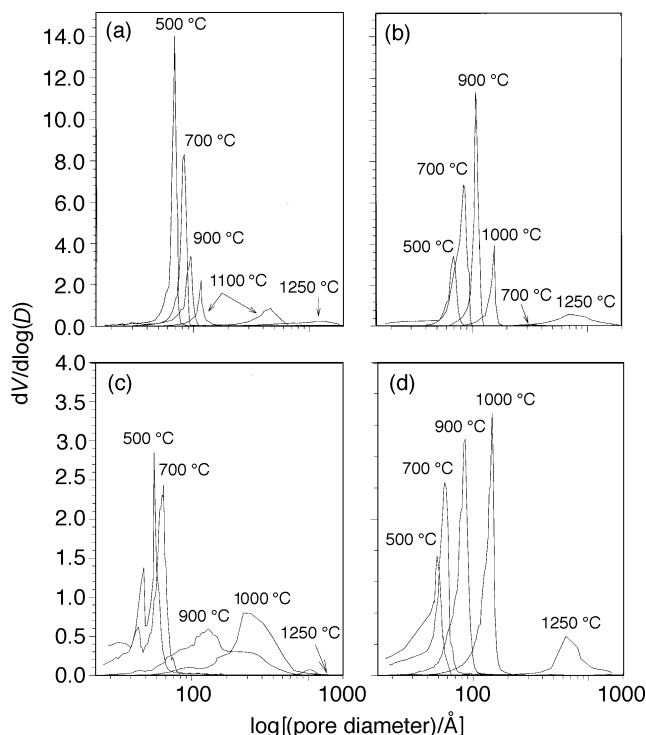
Fig. 2 Pore size distribution of (a) S10A, (b) S9A1B, (c) C10A and (d) C9A1B calcined at different temperatures

PSD of alumina borates showed a lack of any bimodal pore distribution, as would be expected for materials consisting of simply a mixture of two oxides, thereby indicating that these materials are not just physical mixtures of alumina and diboron trioxide. On the other hand, it was found that for samples calcined at lower temperatures, the PSDs were rather narrow. It can also be seen that the PSDs of samples synthesized by the sol–gel process were narrower than those from the coprecipitation method, especially in alumina samples. Finally, according to the saturation adsorption capacity Fig. 1 also suggested a decrease of the total pore volume for calcination at higher temperatures (except for S9A1B at 900 °C and C10A at 700 °C). Obviously, the densification under heating leads simultaneously to widening of the pores and shrinkage of the bulk. There were fewer but generally larger pores after calcination. The porous structure characteristics, including BET surface area, pore size and pore volume, obtained from the conventional analysis of nitrogen isotherms are collected in Table 1. The pore volume of samples obtained from coprecipitation was rather stable upon calcination, until the appearance of the α-alumina crystalline phase. For C10A, thermal densification of coarsened microstructure was accomplished at 1250 °C with the pore size becoming smaller.

It is noteworthy that for C10A, a bimodal PSD was found at 500–700 °C, while at higher calcination temperatures broad PSDs were observed. A low addition of borate (C9A1B) can

lead to the absence of any bimodal distribution, indicating that the presence of borate alters the chemical environment of alumina and changes the structure of alumina as indicated by the solid state NMR results of Peil et al.[21] For S10A, a two-step isotherm was observed for calcination at 1100 °C, leading to a bidisperse pore structure shown in Fig. 2(a). The appearance of different pore sizes can be understood from the XRD patterns shown in Fig. 3(a). The gel was completely amorphous after calcination at 700 °C, but transformed to γ-alumina at 900 °C. α-Alumina appeared at 1100 °C and the transformation was complete at 1250 °C. The bidisperse pore structure observed for the 1100 °C sample thus corresponds to the coexistence of two different solid phases. This phenomenon was also observed for C10A at 500–700 °C. As displayed in Fig. 1(c), a slight two-step adsorption or desorption isotherm corresponds to a bidisperse pore structure shown in Fig. 2(c) and a mixture of α-Al(OH)$_3$, η-Al$_2$O$_3$ and γ-AlOOH, etc. phases [Fig. 3(c)].

Finally, the alkoxide derived alumina xerogels (S10A) display a different crystallization route compared to those obtained from the coprecipitation method, as displayed in Fig. 3. Gibbsite and bayerite phases as well as the θ-Al$_2$O$_3$ phase are all absent in the transformation to α-alumina. Another
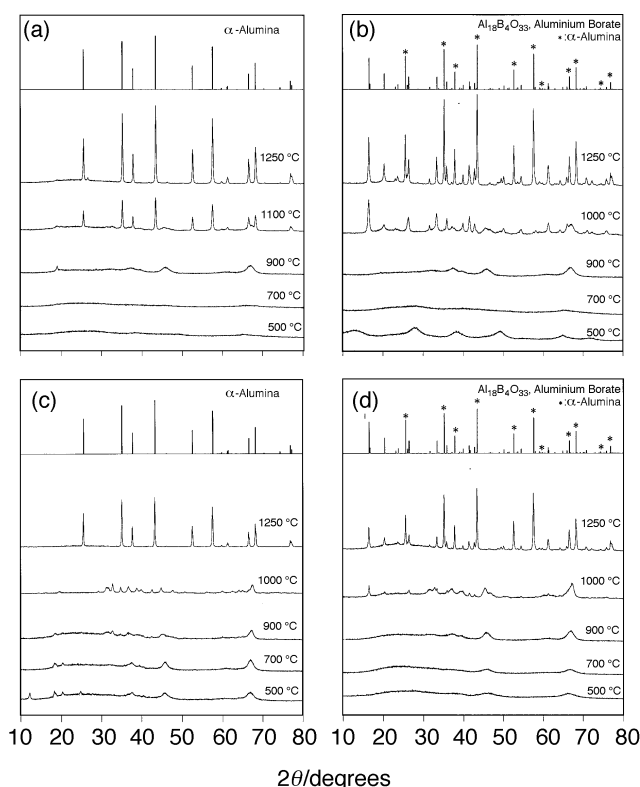

Fig. 3 XRD patterns of (a) S10A, (b) S9A1B, (c) C10A and (d) C9A1B calcined at different temperatures. Also shown are the patterns of pure α-Al$_2$O$_3$ and aluminium borate.

Table 1 Pore structure characteristics of alumina and aluminium borate obtained from conventional analysis of nitrogen isotherms

calcination temperature /°C	S10A			S9A1B			C10A			C9A1B		
	BET/ m² g⁻¹	pore diameter/ Å	pore volume/ cm³ g⁻¹	BET/ m² g⁻¹	pore diameter/ Å	pore volume/ cm³ g⁻¹	BET/ m² g⁻¹	pore diameter/ Å	pore volume/ cm³ g⁻¹	BET/ m² g⁻¹	pore diameter/ Å	pore volume/ cm³ g⁻¹
500	430.8	62.7	0.79	452.5	76.9	0.70	396.8	36.0	0.37	358.1	35.9	0.34
700	311.9	70.7	0.61	343.8	79.5	0.40	310.4	42.3	0.38	286.1	45.7	0.35
900	128.7	80.9	0.35	207.3	104.0	0.71	113.7	119.8	0.36	166.1	74.8	0.37
1000	—	—	—	49.2	137.1	0.24	46.2	255.7	0.36	75.0	123.3	0.31
1100	53.5	—	0.32	—	—	—	—	—	—	—	—	—
1250	8.7	505.8	0.09	9.3	502.6	0.07	4.67	147.8	0.01	20.9	321.8	0.15

interesting feature in Fig. 3 is the continued amorphous nature of coprecipitation derived aluminium borate (C9A1B) at calcination between 500 and 700 °C, whereas upon calcination of C10A in the same temperature range a mixture of alumina hydrates was observed. For sol–gel derived counterparts alumina hydrates existed in S9A1B.

3.2 Pore connectivity: percolation analysis

As shown in Fig. 1, the hysteresis loops formed between the adsorption and desorption branches of the isotherms for the calcined S10A, S9A1B and C9A1B samples belong to IUPAC type H2 loops (except that for the 1250 °C samples, which is a typical H3 loop). Isotherms of C10A are H3 type (900–1250 °C) or of slight two-step nature (500–700 °C), which are difficult to analyze using Seaton theory. On the other hand, it was found that the knee of the hysteresis loops moves to the right and the desorption branch flattens slightly as the calcination temperature increases. According to Seaton theory, if the major contributor to the observed H2 type hysteresis loop is the connectivity of the pore network, this connectivity-related phenomenon may be appropriately described by the percolation process.

Fitting results from the isotherms for the calcined S10A, S9A1B and C9A1B samples are given in Table 2 and Fig. 4–6. The isotherms for 1250 °C samples and the 1100 °C sample of
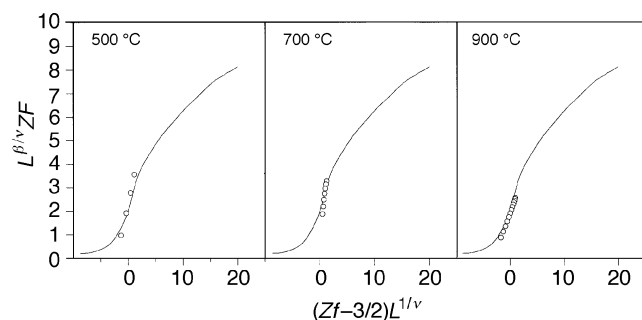
Fig. 4 Fitting of the (f, F) data calculated from the measured isotherms on S10A to that calculated from the generalized relationship (solid line)
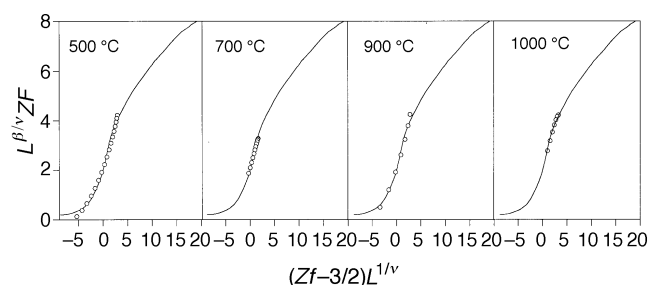
Fig. 5 Fitting of the (f, F) data calculated from the measured isotherms on S9A1B to that calculated from the generalized relationship (solid line)

Table 2 Results of percolation analysis of nitrogen isotherms on S10A, S9A1B and C9A1B

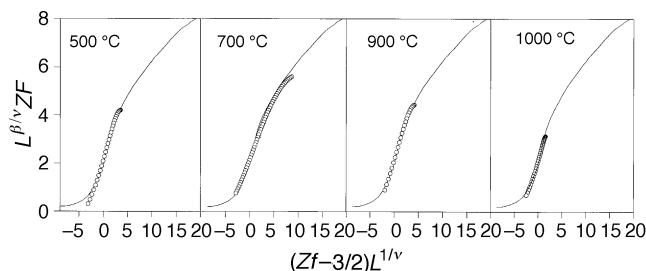| calcination temperature /°C	S10A		S9A1B		C9A1B	
	Z	L	Z	L	Z	L
500	2.1	18.5	1.9	7.3	3.2	4.2
700	2.8	5.2	2.1	3.5	2.6	6.1
900	3.0	2.2	1.8	10.3	2.6	6.6
1000	—	—	2.3	5.0	2.3	2.7

Fig. 6 Fitting of the (f, F) data calculated from the measured isotherms on C9A1B to that calculated from the generalized relationship (solid line)

S10A were excluded either because of the absence of micro- and meso-pores or bimodal pore size distribution.

All the values of Z obtained are in the range 2–3, with a slight increasing (S10A and S9A1B) or decreasing (C9A1B) trend vs. calcination temperature. These are surprisingly low values compared to the values of 5–7 obtained by Seaton[3] for a range of silica and alumina gels. The increase of Z with increasing temperature is readily understood. According to percolation theory, the 'knee' of the desorption isotherm indicated in Fig. 1 corresponds to the percolation threshold. In a highly connected network, it is easier to form a spanning cluster of vapor-filled pores. Once a few pores contain vapor, other pores will be easy to access by the vapor phase. Hence, the location of the desorption 'knee' is more to the right. Accordingly, the isotherms in Fig. 1 suggest a slight increase of pore connectivity with increasing calcination temperature if the hysteresis loop is purely determined by the effect of the pore network. On the other hand, the decrease of Z with increasing temperature is difficult to interpret by this analysis. Since both thermodynamic factors (single-pore mechanism) and pore networks can contribute to the adsorption hysteresis, one explanation is that the hysteresis loop is not uniquely determined by the pore connectivity and the thermodynamic contribution to the adsorption hysteresis is not negligible.

Examination of the Z values of S10A and S9A1B showed that the incorporation of boron into the alumina structure slightly decreases the connectivity of pore network. On the other hand, Z values of C9A1B are larger than those of S9A1B. Since the C9A1B sample obtained from the coprecipitation method consists mainly of aggregates of small primary particles whereas S9A1B synthesized from a low-water non-aqueous solution of alkoxide is a spanned cluster of polycationic polymers of aluminium borate, the above analysis implies that the polymeric aluminium borate gel has a smaller pore connectivity than its colloidal counterpart.

Along with the calculation of Z, values of L are obtained from the fitting. However, it is difficult to link L values to any well defined dimension in the systems. Furthermore, it has been found in our study that the fitting was sensitive to both L and Z values. Hence, the values of L must be taken with some caution.

4 Conclusions

The present study provided well measured nitrogen isotherm data for sol–gel and coprecipitation derived alumina and aluminium borate gels at a variety of calcination temperatures. Percolation analysis was then performed on those nitrogen isotherms to evaluate the value of pore connectivity, Z. Both the alumina and aluminium borate gels showed low pore connectivity with Z values in the range 2–3. The pore connectivity does not change significantly during thermal treatment, despite a large increase in pore size. It was also found that the incorporation of boron into the alumina structure by the

sol–gel process may decrease the pore connectivity. On the other hand, Z values of sol–gel derived samples differ from those of samples obtained by coprecipitation, indicating that the pore connectivity of materials obtained from polymeric and colloidal mechanisms is different.

These results confirm that it is helpful to use percolation analysis for comparative studies of changes of the initial pore structure of porous materials, caused by a particular treatment or modification. Since this method needs no extra data except the nitrogen isotherms or mercury penetration curves, such analysis can be viewed as an additional standard technique.

References

1 J. Rouquerol, D. Avnir, C. W. Fairbridge, D. H. Everett, J. H. Haynes, N. Pernicone, J. D. F. Ramsay, K. S. W. Sing and K. K. Unger, *Pure Appl. Chem.*, 1994, **66**, 739.
2 C. K. Lee, A. S. T. Chiang and C. S. Tsay, in *Key Engineering Materials*, ed. D.-M. Liu, Trans Tech Publications, Switzerland, 1996, vol. 115, p. 21.
3 N. A. Seaton, *Chem. Eng. Sci.*, 1991, **46**, 1895.
4 H. Liu, L. Zhang and N. A. Seaton, *Chem. Eng. Sci.*, 1992, **47**, 4393.
5 H. Liu, L. Zhang and N. A. Seaton, *J. Colloid Interface Sci.*, 1993, **156**, 285.
6 H. Liu, L. Zhang and N. A. Seaton, *Langmuir*, 1993, **9**, 2576.
7 H. Liu and N. A. Seaton, *Chem. Eng. Sci.*, 1994, **49**, 1869.
8 E. P. Barrett, L. G. Joyner and P. H. Halenda, *J. Am. Chem. Soc.*, 1951, **73**, 373.
9 S. Kirkpatrick, in *III-Condensed Matter*, ed. R. Balian, R. Mayward and G. Toulouse, North-Holland, Amsterdam, 1979, p. 324.
10 J. Livage, *Solid State Ionics*, 1996, **86-88**, 935.
11 S. Suda, K. Yamashita and T. Umegaki, *Solid State Ionics*, 1996, **89**, 75.
12 C. A. Browne, D. H. Tarrant, M. S. Olteanu, J. W. Mullens and E. L. Chronister, *Anal. Chem.*, 1996, **68**, 2289.
13 K. Kuraoka, H. Tanaka and T. Yazawa, *J. Mater. Sci. Lett.*, 1996, **15**, 1.
14 T. Skapin and E. Kemnitz, *Catal. Lett.*, 1996, **40**, 241.
15 M. C. Tsai and Y. W. Chen, *Catal. Lett.*, 1990, **6**, 225.
16 B. E. Yoldas, *Am. Ceram. Soc. Bull.*, 1975, **54**, 286.
17 S. J. Wilson and M. H. Stacey, *J. Colloid Interface Sci.*, 1981, **82**, 507.
18 V. Saraswati, G. V. N. Rao and G. V. R. Rao, *J. Mater. Sci.*, 1987, **22**, 2529.
19 A. Ayral and J. Phalippou, *Adv. Ceram. Mater.*, 1988, **3**, 575.
20 G. V. R. Rao, S. Venkadesan and V. Sarawati, *J. Non-Cryst. Solids*, 1989, **111**, 103.
21 K. P. Peil, L. G. Galya and G. Marcelin, *J. Catal.*, 1989, **115**, 441.
22 B. E. Yoldas, in *Ultrastructure Processing Advanced Ceramic*, ed. J. D. Mackenzie and D. R. Ulrich, Wiley & Sons, New York, 1988, p. 333.
23 C. S. Tsay, C. K. Lee and A. S. T. Chiang, *Chem. Phys. Lett.*, 1997, **278**, 83.